NeuroImage 328 (2026) 121775

Contents lists available at ScienceDirect

NeuroImage

journal homepage: www.elsevier.com/locate/ynimg

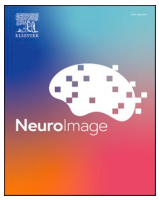

Morphometric dissimilarity in association cortices linked to autism subtype with more severe symptoms

Hongxiu Jiang [a,*], Raul Rodriguez-Cruces [a], Ke Xie [a], Valeria Kebets [a], Yezhou Wang [a], Clara F. Weber [a,b,c], Ying He [a], Jonah Kember [a], Hilary Sweatman [a], Zeus Gracia Tabuenca [d], Jean-Baptiste Poline [a], Danilo Bzdok [a], Seok-Jun Hong [e,f], Boris Bernhardt [a], Xiaoqian Chai [a]

[a] McConnell Imaging Center, Montreal Neurological Institute, McGill University, Montreal, Quebec, Canada
[b] Social Neuroscience Lab, Department of Psychiatry and Psychotherapy, University of Lübeck, Lübeck, Schleswig-Holstein, Germany
[c] Center of Brain, Behavior and Metabolism (CBBM), University of Lübeck, Lübeck, Germany
[d] Department of Statistical Methods, University of Zaragoza, Zaragoza, Spain
[e] Center for Neuroscience Imaging Research, Institute for Basic Science (IBS), Suwon, South Korea
[f] Department of Biomedical Engineering, Sungkyunkwan University, Suwon, South Korea

ARTICLE INFO

Keywords:
Autism spectrum disorder
Morphometric similarity networks
Subtypes
Structural MRI

ABSTRACT

Autism spectrum disorder (ASD) is a prevalent and heterogeneous neurodevelopmental condition marked by atypical brain connectivity. Understanding ASD neural subtypes at the network level is critical for clarifying its neuroanatomical heterogeneity. Morphometric similarity networks (MSNs), derived from region-to-region similarity across multiple anatomical features, offer a powerful approach for capturing individual-level neural architecture. In this study, MSNs were estimated from seven anatomical features in 348 individuals with ASD and 452 typically developing (TD) controls. Across all ASD participants, the first principal component of MSN values was negatively correlated with social and communication severity. Three ASD subtypes with distinct MSN patterns were identified. Subtype-1, characterized by weaker morphometric similarity values in frontotemporal association regions compared to TD individuals, exhibited the most severe symptoms in social, communication and repetitive behaviors, and displayed hyperconnectivity between the salience and visual networks, and between language and visual networks. Subtype-2 showed greater values of morphometric similarities than TD and less severe social symptoms compared to subtype-1, along with hyperconnectivity between default and salience networks relative to TD. Subtype-3 displayed morphometric similarity values largely comparable to TD and the least severe symptoms out of the three subtypes. Transcriptomic analysis revealed that GABAergic parvalbumin and glutamatergic intratelencephalic-projecting neurons were key cell types differentiating subtypes. These findings suggest the existence of distinct ASD neuroanatomical subtypes defined by regional morphometric similarity, each linked to unique behavioral, functional, and transcriptomic profiles. Morphometric dissimilarity in association regions may serve as a neural signature for ASD subtypes characterized by more severe clinical manifestations.

1. Introduction

Autism spectrum disorder (ASD) is a prevalent developmental condition characterized by impairments in social, communication, restricted interests and repetitive behaviors. Among ASD individuals, there is great variability in both behavioral patterns and underlying biological substrates (London, 2014). Although important progress has been made over the past decades on the neuroanatomical and functional bases of ASD using brain imaging methods such as magnetic resonance imaging (MRI), inconsistent findings are often reported when comparing individuals with ASD to those who are not autistic (termed typically developing, or TD) (Hyde et al., 2010; Chen et al., 2011; Khundrakpam et al., 2017; Pua et al., 2017). Multiple factors may contribute to the inconsistent findings reported across structural MRI studies in ASD. These include methodological differences—such as the choice of morphometric features (e.g., cortical thickness, surface area and gray

* Corresponding author.
E-mail address: jhx201001@gmail.com (H. Jiang).

https://doi.org/10.1016/j.neuroimage.2026.121775
Received 7 August 2025; Received in revised form 30 January 2026; Accepted 3 February 2026
Available online 4 February 2026

matter volume), differences in statistical modeling and confound adjustment strategies (e.g., whether age, sex, IQ, site, or motion are controlled), and network construction approaches (structural covariance and diffusion tractography)—as well as variability in preprocessing strategies and scanner characteristics across sites (Cruz Puerto and Sandín Vázquez, 2024). In addition, differences in sample composition (e.g., age range, sex distribution, IQ profile) may further contribute to variability (Lenroot and Yeung, 2013; Lombardo et al., 2019). Importantly, heterogeneity in the underlying brain organization in ASD might be a main contributor of these inconsistencies.

To address this, several studies have used data-driven strategies to identify subgroups of ASD with shared common brain structural and/or functional patterns. For example, ASD subtypes have been identified using isolated anatomical features, including grey matter volume (Chen et al., 2019) and cortical thickness (Zabihi et al., 2020) or multiple composites (Hong et al., 2018), revealing preliminary evidence for structural MRI-based ASD subtypes. However, ASD is increasingly recognized as a condition characterized by atypical brain connectivity (Valk et al., 2015; Chen et al., 2017; Carroll et al., 2021), underscoring the importance of considering the relationships among different brain regions.

There has been a shift toward network-level subtyping to better capture the distributed nature of ASD neurobiology. Several studies have used whole-brain resting-state functional connectivity (FC) to derive ASD subgroups. For example, Easson et al. (2019) identified two FC-based subtypes distinguished by the balance between within-network and between-network connectivity. Choi et al. (2022) and Guo et al. (2022) have incorporated individualized FC patterns or diagnostic information into the clustering process, revealing neuro-subtypes with distinct connectivity features and symptom profiles. Building on these functional connectivity–based subtyping efforts, examining ASD subtypes from the perspective of structural brain network organization offers an alternative and complementary framework for characterizing distributed neuroanatomical variation across individuals. Accordingly, investigating subtypes based on structural brain network organization is essential to investigate subtypes based on structural brain network organization.

Structural network approaches—including structural covariance networks (SCN) and diffusion tensor imaging (DTI)—have also implicated altered network communication in ASD. Disruption of SCN has been reported in ASD in language (Sharda et al., 2016), social and sensory-processing regions (Balardin et al., 2015). Reduced coherence of the white matter microstructures accessed by DTI has been reported in ASD (Dean III et al., 2016). However, both approaches have limitations for investigating neuroanatomical heterogeneities in ASD. Traditional structural covariance network (SCN) approaches are typically constructed using a single morphometric feature and characterize inter-regional covariance patterns, rather than explicitly modeling multi-feature structural relationships within individuals. Meanwhile, mapping the structural connectome using DTI tractography is challenging due to the fundamental ambiguities inherent in tract reconstruction, which affects the reliability and accuracy of the findings.

Morphometric Similarity Networks (MSNs), introduced by Seidlitz et al. (2018), provide a powerful alternative for individual-level structural connectomics. MSNs leverage multiple structural features [e.g.: gray matter volume, surface area and cortical thickness] to quantify the morphometric similarity between regions, which has been linked to cytoarchitectonic similarity, axonal connectivity, and gene co-expression patterns (Seidlitz et al., 2018). Regions with higher morphometric similarity are more likely to belong to the same cytoarchitectonic type. This approach is grounded in animal research, which suggests regions with similar laminar structure and cellular composition have greater connectivity through axonal tracts (Goulas et al., 2017). Further supporting the validity of MSN as a structural connectivity measure, MSN from the macaque monkey is closely correlated with networks based on axonal tract tracing (Seidlitz et al., 2018). Therefore, MSN has been proposed to be a proxy of axonal connectivity (Sebenius et al., 2024). Although not a direct measure of axonal or functional connectivity, MSN structure has been shown to align with patterns of cytoarchitecture, gene expression, and tracer-based anatomical connectivity (Cao et al., 2023), thereby providing a morphology-based analogue of large-scale network organization. Moreover, MSN topology has also been shown to reflect individual differences in cognitive measures (Vuksanović, 2022). Research on MSN in typically developing individuals has revealed valuable insights into the cognitive and affective development in the brain. Whole-brain MSN measured in newborns can be predictive of social-emotional performance at 18 months (Fenchel et al., 2022). During adolescence, morphometric similarity increases in paralimbic cortical areas such as the insula and cingulate cortex and decreases in neocortical regions (Dorfschmidt et al., 2024). Morphometric similarity of brain modules in pre-adolescents has been linked to psychiatric problem scores (Wu et al., 2023). Despite these advances in understanding typical development, MSN can also be harnessed to uncover biological mechanisms in ASD. For instance, Del Casale et al. (2025) reported significant alterations in both global and regional brain network organization in ASD, while finding no significant associations between ASD severity and connectivity indices. Given that ASD is a neurodevelopmental disorder with high neurobiological heterogeneity, identifying meaningful subtypes by using morphometric similarity networks may be beneficial to explore associations between behavior and brain imaging in ASD.

Here, we investigated ASD subtypes based on MSN and examined their associated functional connectivity patterns and genetic signatures. First, individual MSN matrices were constructed, then hierarchical clustering combined with bootstrapped-based stability assessments was used to identify ASD subtypes. Second, we examined clinical symptom profiles and resting-state functional connectivity patterns across the identified subtypes. Third, we employed partial least squares regression (PLSR, Wold (1966)) to explore the relationship between subtype-specific MSN differences and genetic signatures from the Allen Human Brain Atlas. We further conducted functional enrichment and cell-type enrichment analyses. We hypothesized that MSN values would be associated with ASD symptom severity, and that each subtype would exhibit distinct functional connectivity and genetic patterns.

2. Methods

2.1. Subjects

Due to the high ASD incidence in male individuals and the number of subjects, this study included only male participants. T1-weighted scans were used from 12 sites across 3 datasets, including the Autism Brain Imaging Data Exchange (ABIDE) (Di Martino et al., 2014, 2017), the Province of Ontario Neurodevelopmental (POND) Network, and the Human Connectome Project in Development (HCP-D) (Somerville et al., 2018). Specifically, subjects were selected based on the following inclusion criteria: (1) male; (2) acceptable structural MRI quality, as determined by visual inspection of T1-weighted images for motion artifacts; (3) acceptable functional MRI quality (see details in **2.2** section).

All data collection procedures were approved by the local ethics committee on each dataset. For ABIDE, data was fully anonymized and the research ethics boards were Barrow Neurological Institute, Kennedy Krieger Institute, New York University Langone Medical Center, Oregon Health and Science University, San Diego State University, University of Pittsburgh School of Medicine, and University of Utah School of Medicine. For POND, the research ethics boards were University of Toronto, Holland Bloorview Kids Rehabilitation Hospital, Hospital for Sick Children, McMaster University, McMaster Children's Hospital, Mohawk College, Western University, Children's Hospital at London Health Sciences Centre, Lawson Health Research Institute, Queen's University, Ongwanada Resource Center, and Hotel Dieu Hospital. For HCP-D,

written informed consent was obtained from all participants, with a parent or legal guardian providing written permission for participants under 18 years of age, and the research ethics boards were Harvard University, University of California-Los Angeles, University of Minnesota, and Washington University in St. Louis.

The final sample included 348 individuals with ASD and 452 TD. The two groups were matched in age (ASD: mean = 12.79, standard deviation (std) = 4.24, range = 5 – 23; TD: mean = 13.19, std = 4.11, range = 5 – 23; $t = -1.35$, $p = 0.273$). Compared to TD, individuals with ASD had significantly lower full-scale IQ compared to TD (ASD: mean = 101.40, std = 18.99, range = 40 - 148; TD: mean = 111.93, std = 13.61, range = 53 - 144; $t = -7.38$, $p < 0.001$).

2.2. MRI preprocessing and functional connectivity construction

T1w MRI images were processed using FreeSurfer (v6.0, https://surfer.nmr.mgh.harvard.edu/). Standard preprocessing steps, including skull-stripping, bias field correction, registration, anatomical segmentation, and surface reconstruction, were applied to structural images. The cortical surfaces were divided into 308 regions (Romero-Garcia et al., 2012) by further subdividing the original 68 cortical regions in the Desikan–Killiany atlas (Desikan et al., 2006) into spatially contiguous parcels of approximately 500 mm^2 in surface area. For each region, seven morphometric features were employed in the MSN construction (see below for details): gray matter volume (GM), mean cortical thickness (CT), surface area (SA), mean curvature (MC), Gaussian curvature (GC), curvature index (CI), and fold index (FI) (Li et al., 2017).

Rs-fMRI data were processed and analyzed using the CONN-fMRI Functional Connectivity toolbox v20b (Whitfield-Gabrieli and Nieto-Castanon, 2012), MATLAB R2021b. Preprocessing followed the default CONN pipeline, including: functional label current files as "original data", functional realignment and unwarp, functional center to (0,0,0) coordinates, functional outlier detection (Artifact Detection Tools was used to identify the outlier scans for scrubbing), structural center to (0,0,0) coordinates, functional indirect segmentation and normalization, functional label current files as "MNI-space data", and functional smoothing (spatial 8-mm Gaussian kernel). Data were denoised using the following steps: signal from the cerebrospinal fluid and white matter estimated by aCompCor (Behzadi et al., 2007; Chai et al., 2012) were regressed out, a bandpass filter (0.008–0.09 Hz) was applied, to reduce the noise effects from physiological effects and scanner drift. In the first-level analysis, realignment parameters and motion outlier regressions were included as covariates.

We carried out ROI-ROI connectivity analyses to characterize

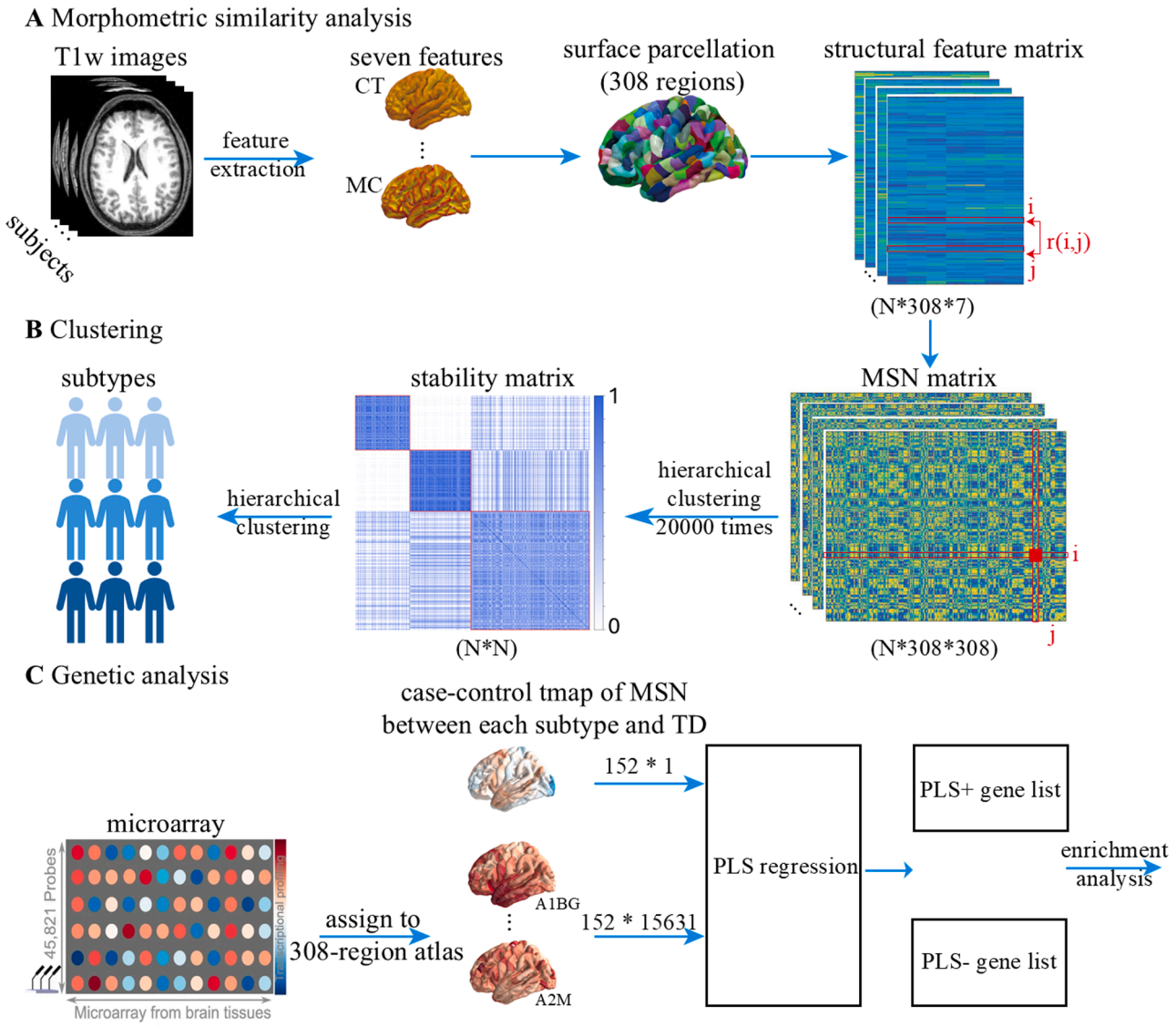

Fig. 1. Methods overview. **A.** Structural feature extraction and morphometric similarity network construction. **B.** The clustering process. **C.** Genetic analysis.

subtype-specific connectivity patterns. Thirty-two independent components derived from ICA decomposition of the Human Connectome Project (HCP) dataset, available within CONN, were used as ROIs (Calhoun et al., 2001). The mean time series of each ROI was extracted, and Pearson correlation coefficients were calculated between all ROI pairs. These values were then transformed using Fisher's r-to-z transformation for statistical analysis.

2.3. Morphometric similarity network construction

In each participant, the MSN was constructed by calculating Pearson correlation for each pair of z-normalized morphometric feature vectors consisting of the seven morphometric features of different regions, forming a 308 × 308 matrix for each participant (Seidlitz et al., 2018), as shown in Fig. 1A. Next, a mean regional MSN was computed by averaging the values in each row of the matrix, yielding a 308-element vector for each subject. Higher mean regional MSN values indicate that a region shares a more similar multi-feature morphometric profile with widespread cortical territories (i.e., greater global structural embedding), whereas lower values reflect more differentiated, region-specific morphometric patterns. While this metric is conceptually analogous to global connectivity or degree centrality in diffusion- and functional-based networks, it captures morphometric similarity rather than direct axonal or functional coupling. Thus, mean regional MSN provides a morphology-based analogue of global network embedding that complements traditional measures of structural and functional connectivity. NeuroCombat (Fortin et al., 2018) was used to adjust for scanner/site effects by harmonizing the mean and variance of brain measures across sites. Subsequently, we performed a linear regression model (LRM) to account for the effect of age, and used the residuals of this model as the corrected mean regional MSN values for subsequent analyses.

2.4. Relating MSN values to ASD symptom scores

To assess whether MSN values are related to ASD symptoms, we used principal component analysis (PCA, Wold et al. (1987)) and Pearson correlation to quantify the relation between mean MSN values and clinical scores measured by ADI-R. Specifically, we first run PCA on the mean MSN matrix of the ASD group with a dimension of $N \times 308$, where N was the number of individuals with ASD. The first principal component was extracted and correlated with ADI-R symptom scores using Pearson correlation.

2.5. Clustering analysis

Hierarchical clustering (Bridges Jr, 1966) was applied to the MSN features. Clustering performance was evaluated using the silhouette coefficient (Rousseeuw, 1987), with the number of clusters (k) ranging from 2 to 10. The silhouette value, ranging from −1 to +1, quantifies

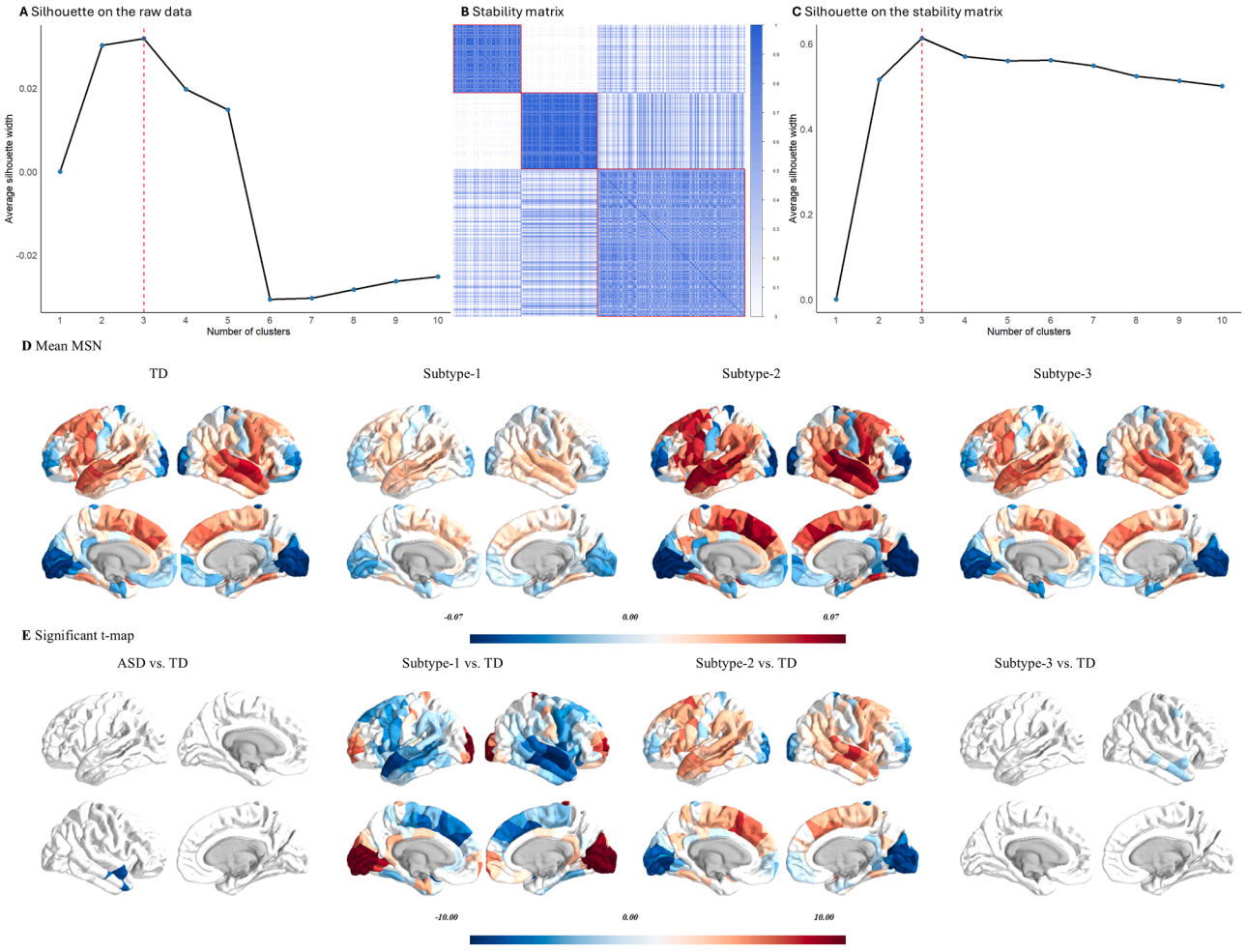

Fig. 2. Clustering indices, individual-level patterns, and case-control differences in mean regional morphometric similarity networks (MSNs). A. Silhouette values computed from the $N \times 308$ MSN matrix. B. Stability matrix obtained from 20,000 clustering iterations. C. Silhouette values based on the stability matrix. D. Mean regional MSN for each group (TD and ASD subtypes). E. Significant group differences in mean regional MSN (TD vs. ASD), displayed as a t-map corrected for multiple comparisons using FDR. TD, typically developing; MSN, morphometric similarity network.

how similar an individual is to its assigned cluster relative to other clusters; higher values indicate better clustering quality. We observed the highest silhouette score at $k = 3$ (Fig. 2A) and thus selected this as the optimal number of clusters.

To obtain stable subtyping results, we carried out 20,000 iterations of bootstrapping and constructed the stability matrices (Rodríguez-Cruces et al., 2020). In each bootstrapping iteration, a binary $N \times N$ stability matrix was generated (N = *the number of subjects*), where a value of 1 indicates that a pair of subjects was assigned to the same cluster, and 0 indicates otherwise. The final stability matrix was computed by averaging across all bootstrap iterations, capturing the probability that any pair of individuals was consistently clustered together, as shown in Fig. 2B. We further confirmed that $k = 3$ yielded the highest silhouette score when applied to the final stability matrix (Fig. 2C). This bootstrap-based approach enabled the identification of stable ASD subgroups characterized by distinct MSN profiles.

Due to the limited number of subjects, we chose to use this bootstrapping/similarity matrix approach to maximize stability of the clustering, rather than including a replication dataset. We believe this approach is a better and sound alternative that addresses generalizability for the data available.

2.6. Group comparison analyses in symptom scores and functional connectivity

To compare MSN maps between each subtype and TD, we ran two-sample *t*-test on the corrected mean regional MSN for each region. Differences in symptom scores between subtypes were tested using a one-way analysis of covariance (ANOVA), implemented with the *aov* function in R, with a significance level of $p < 0.05$. Post hoc two-sample *t*-test was used for pairwise comparisons between specific subtypes. FC differences between each subtype and the TD group were examined using two-sample *t*-tests while controlling for age and site, with a threshold of $p < 0.01$. False discovery rate (FDR) (Benjamini and Hochberg, 1995) was used for all comparisons.

2.7. Regional gene expression matrix

Transcriptomic data were obtained from the Allen Human Brain Atlas (AHBA, http://human.brain-map.org/, Hawrylycz et al. (2012)), which includes a whole-genome expression atlas from 6 postmortem donors (age = 42.50 ± 13.38; male/female = 5/1). The *Abagen* toolbox (Markello et al., 2021) was used to preprocess the transcriptomic data. In brief, genetic probes were reannotated using updated information provided by Arnatkevičiūtė et al. (2019) to remove probes with less reliability rather than the default provided by from AHBA dataset. The reannotated probes were kept only when their intensity related to the background noise level was larger than 50%. The microarray expression data were normalized and aggregated (Markello et al., 2021) to the above-mentioned 308-region parcellation. Because genetic data was only available from two right hemispheres, this study analyzed the left hemisphere only with 152 regions. These steps result in the gene expression matrix with a dimension of 152 × 15, 631 for the analysis.

2.8. Linking MSN to gene expression in ASD subtypes

To examine transcriptomic associations with MSN differences, we performed PLSR using *plsregress* in MATLAB, as shown in Fig. 1C. The gene expression matrix (152 regions × 15,631 genes) served as the predictor, while the t-statistic map of MSN differences (ASD subtype vs. TD) in 152 left hemisphere regions served as the response variable. PLSR analysis decomposes the predictor to create orthogonal components that can best predict the response variables. We focused on the first component of PLSR (PLSR1), as it explains most of the variance. A permutation test was further used to test the statistical significance of the variance explained by PLSR1, where the spatial permutation models generate spatial-constrained null distributions by applying random rotation to spherical projections of the brain (Alexander-Bloch et al., 2018). Bootstrapping was used to estimate the variability of PLSR1 of each gene, with the Z score of the ratio of the weight of each gene to the standard error of bootstrap as the criterion for ranking their contributions to PLSR1.

2.9. Enrichment analysis of genes transcriptionally related to regional changes

Genes ranked by PLSR1 loadings were submitted for functional enrichment analysis using Metascape (Zhou et al., 2019), covering gene ontology (GO) biological processes, Kyoto Encyclopedia of Genes and Genomes (KEGG) pathways, Reactome Genes Sets and WikiPathways. Additionally, expression-weighted cell type enrichment (EWCE, Skene and Grant (2016)) was performed to identify differences in cell-type associations between subtypes, using the PLSR1-ranked gene lists as input.

3. Results

3.1. MSN-behavior relationships

In the ASD group, there are 254 individuals who have ADI-R RRB (restricted, repetitive, and stereotyped behaviors and interests) subscore, and 252 individuals have ADI-R communication (language/communication) and social (reciprocal social interactions) subscores. We found significant negative correlations between the first component (PC1) of the mean MSN matrix and ADI-R communication ($r = -0.16$, $p = 0.011$), and social subscore ($r = -0.15$, $p = 0.020$), as shown in **Fig. S1A**.

Regional loading pattern of PC1 was projected onto the cortical surface in **Fig. S1B**. Positive loadings were predominantly located in lateral occipital and frontal pole regions, whereas negative loadings were concentrated in frontotemporal and insular association cortices. This spatial pattern demonstrates that PC1 captures a large-scale structural gradient spanning association to sensory–perceptual systems. Given the negative association between PC1 scores and ADI-R symptom severity, lower PC1 scores—reflecting reduced morphometric similarity in frontotemporal association cortices—correspond to more pronounced social and communicative symptoms in ASD. These findings suggest that weaker MSN values (morphometric dissimilarity) were associated with increased severity of core ASD symptoms.

3.2. Altered MSN in three ASD subtypes

We identified three subtypes of ASD based on hierarchical clustering of MSN values. The clustering index and stability matrix are presented in Fig. 2A-C, and the mean regional MSN of the TD group and each ASD subtype are shown in Fig. 2D The group-level mean MSN map of the TD group was consistent with previous studies (Morgan et al., 2019; Li et al., 2021). Specifically, higher morphometric similarity (positive mean regional MSN values) was observed in frontal temporal association cortices, including the caudal middle frontal, superior frontal, superior temporal, and middle temporal regions. In contrast, lower morphometric similarity (negative mean regional MSN values) was evident in visual areas, such as the lateral occipital and lingual cortices, as well as the rostral middle frontal cortex. These patterns suggest that association cortices are more structurally integrated, while visual regions are more differentiated.

To assess inter-individual variability within the TD group, we computed the standard deviation of mean regional MSN values across TD participants and projected this variability onto the cortical surface (Supplementary **Fig. S2**). Inter-individual variability is slightly higher in transmodal association cortices—an expected feature of typical development—while primary sensory regions especially the visual regions

show the lowest variability. Subtype-1 ($N = 81$) and subtype-2 ($N = 91$) exhibited distinct deviations from the MSN pattern of TD in the above-mentioned regions. Compared to TD, subtype-1 had lower values in association regions where the MSN values of TD were positive (e.g., temporal and frontal regions), and less negative values in visual regions where the TD values were negative (e.g., occipital cortex). Conversely, subtype-2 had the opposite pattern in these regions, i.e., more positive MSN values in regions with positive values in TDs and more negative values in regions with negative values in TD. Subtype-3 ($N = 176$) was largely similar to TD, except for five regions – including three in the right middle temporal cortex, one in the superior temporal cortex, and one in the precentral cortex – that exhibited lower MSN values than TD. These subtype-specific alterations were confirmed by two-sample *t*-tests comparing each subtype with the TD group (Fig. 2E), highlighting the spatially distinct morphometric signatures across ASD subtypes.

3.3. Clinical symptom severity across three ASD subtypes

Fig. 3 showed the distribution of ADI-R scores across the three subtypes. Significant differences were observed in the ADI-R communication ($F(2, 248) = 4.48$, $p = 0.012$), RRB ($F(2, 250) = 3.95$, $p = 0.021$) and social ($F(2, 248) = 3.09$, $p = 0.047$) subscales. To further examine these effects, post-hoc two-sample *t*-tests were conducted. The results revealed that subtype-1 exhibited significantly higher scores than subtype-3 on both the ADI-R communication ($t(140.32) = 3.19$, $p = 0.001$) and RRB ($t(114.64) = 2.63$, $p = 0.020$) subscales. Additionally, subtype-1 showed significantly higher ADI-R social scores than subtype-2 ($t(121.27) = 2.50$, $p = 0.041$). These findings suggest that subtype-1 presents more severe impairments across all three symptom domains as measured by the ADI-R.

Table 1 listed the detailed demographic and clinical characteristics of the three ASD subtypes. The table reports group-level information for age, sex distribution, IQ, head motion, ADI-R and ADOS symptom scores (communication, social interaction, and restricted/repetitive behaviors). However, information on race/ethnicity was not available in the ABIDE dataset and therefore could not be included. In this study, we use the term Communication to refer specifically to verbal communication in both ADI-R and ADOS scores.

To ensure that nuisance variables did not drive the subtype solution, we further compared the three subtypes on age and site. An ANOVA revealed no significant age differences among the subtypes ($F(1, 346) = 0.03$, $p = 0.86$). A chi-square test with Monte Carlo simulation (10,000 replicates) similarly indicated no significant site differences among the subtypes ($\chi^2 = 26.49$, $p = 0.14$). These results suggest that potential nuisance factors did not materially account for the identified subtype patterns.

3.4. Atypical functional connectivity patterns of three ASD subtypes

To further examine the distinctions among ASD subtypes, we compared functional connectivity patterns between each subtype and typically developing ($N = 433$) individuals using pairwise ROI-to-ROI analyses in CONN. As shown in **Fig. S3**, subtype-1 ($N = 72$) exhibited hyperconnectivity between the salience and visual networks, and between the language and visual networks. Subtype-2 ($N = 81$) showed increased connectivity between the default and salience networks. In contrast, Subtype-3 ($N = 164$) did not differ significantly from TD in any functional connections.

3.5. Transcriptional profile related to the change of MSN

The genetic data from AHBA were preprocessed and generated a 152 × 15,631 cortical gene expression matrix. We then used PLSR to explore the relationship between the case-control MSN maps and the gene expression matrix for each of the three subtypes. PLSR1 was defined as the spatial map that captured the greatest fraction of total gene expression variance across cortical areas. PLSR1 accounted for 76.4%, 69.0%, and 51.0% of the variance for subtypes-1, 2, and 3, respectively. The PLSR1 weighted gene expression map was significantly spatially correlated with the case-control t-map with Pearson Correlation coefficient ($r = 0.71$, $r = 0.67$, and $r = 0.46$ respectively, Fig. 4A). These positive correlations suggest that genes positively weighted on PLSR1 are overexpressed in regions where morphometric similarity was increased in individuals with ASD compared to TD, while negatively weighted genes are overexpressed in regions where morphometric similarity was decreased in individuals with ASD compared to TD.

We ranked the normalized weights from the PLSR1 using a univariate one-sample Z-test and identified 2511 genes ($Z > 5$) for subtype-1, 2006 genes for subtype-2, and 629 genes for subtype-3. Fig. 4B displayed the top ten significantly enriched genetic pathways and biological processes for each subtype. Genes associated with subtype-1 were primarily enriched in DNA and mRNA metabolic processes and chromosome organization. Subtype-2 genes were mainly involved in synaptic signaling, axon guidance, and neuronal system pathways. In contrast, subtype-3 genes were predominantly related to intracellular receptor signaling pathways, circadian rhythm, and monoatomic cation transmembrane transport.

We conducted expression-weighted cell type enrichment analysis to identify cell types associated with the genes specific to each subtype, as presented in Fig. 4C. Subtype-1 showed significant enrichment in both GABAergic and glutamatergic neurons, with the strongest enrichment observed in GABAergic parvalbumin (PVALB) neurons and glutamatergic L4_IT and L6_CT neurons. Subtype-2 was enriched in GABAergic PAX6 neurons, as well as in glutamatergic IT, L5_6_IT_Car3 and L6b. Subtype-3 exhibited more selective enrichment, prominently involving GABAergic PVALB and glutamatergic L4_IT neurons. Notably, across the three subtypes, the most distinct differences in cell types enrichment were observed in GABAergic PVALB, glutamatergic L4_IT and L6b neurons. These findings highlight subtype-specific patterns of excitatory and inhibitory circuits. **Table S1** provides a brief function description of these neurons.

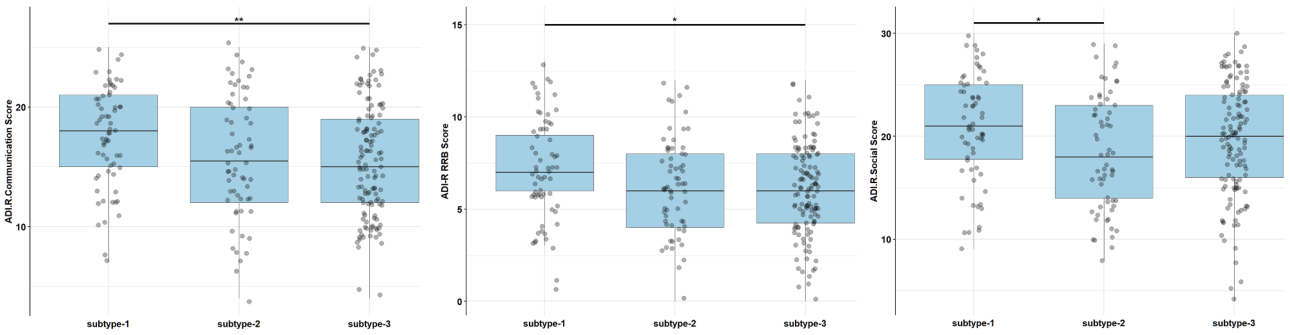

Fig. 3. Behavioral Differences Among ASD Subtypes. * represents $p < 0.05$, **represents $p < 0.01$ (FDR corrected).

Table 1
Demographic and clinical characteristics of subtypes.

	subtype-1		subtype-2		subtype-3		F statistic (*p*-value)	post-hoc
	mean (std)	N	mean (std)	N	mean (std)	N		
Age	12.56 (4.31)	81	13.07 (4.12)	91	12.74 (4.30)	176	0.03 (0.86)	
head motion	0.29 (0.27)	79	0.25 (0.23)	90	0.28 (0.24)	175	0.60 (0.55)	
Full IQ	102.47 (19.89)	74	102.34 (17.73)	86	100.45 (19.33)	168	0.73 (0.39)	
Verbal IQ	94.81 (18.14)	54	100.36 (18.58)	67	97.72 (20.78)	123	0.37 (0.54)	
Performance IQ	102.60 (21.09)	55	104.61 (19.64)	67	101.76 (19.95)	123	0.20 (0.66)	
ADI-R Communication	17.53 (4.17)	64	15.84 (5.15)	62	15.40 (4.67)	125	8.16 (**0.005**)	**subtype-1>subtype-3**
ADI-R RRB	7.20 (2.80)	64	6.24 (2.59)	63	6.11 (2.50)	126	6.69 (**0.01**)	**subtype-1>subtype-3**
ADI-R Social	20.81 (5.24)	64	18.38 (5.62)	61	19.63 (5.52)	126	1.08 (0.30)	
ADOS Communication	3.97 (1.50)	36	3.70 (1.79)	46	3.55 (1.55)	74	1.59 (0.21)	
ADOS RRB	2.39 (1.36)	36	2.17 (1.72)	46	2.20 (1.53)	75	0.28 (0.60)	
ADOS Social	8.28 (2.73)	36	8.50 (2.90)	46	7.63 (2.44)	75	2.16 (0.14)	

Abbreviation: std, standard deviation; ADI-R, Autism Diagnostic Interview–Revised.
N represents the number of subjects with available data.

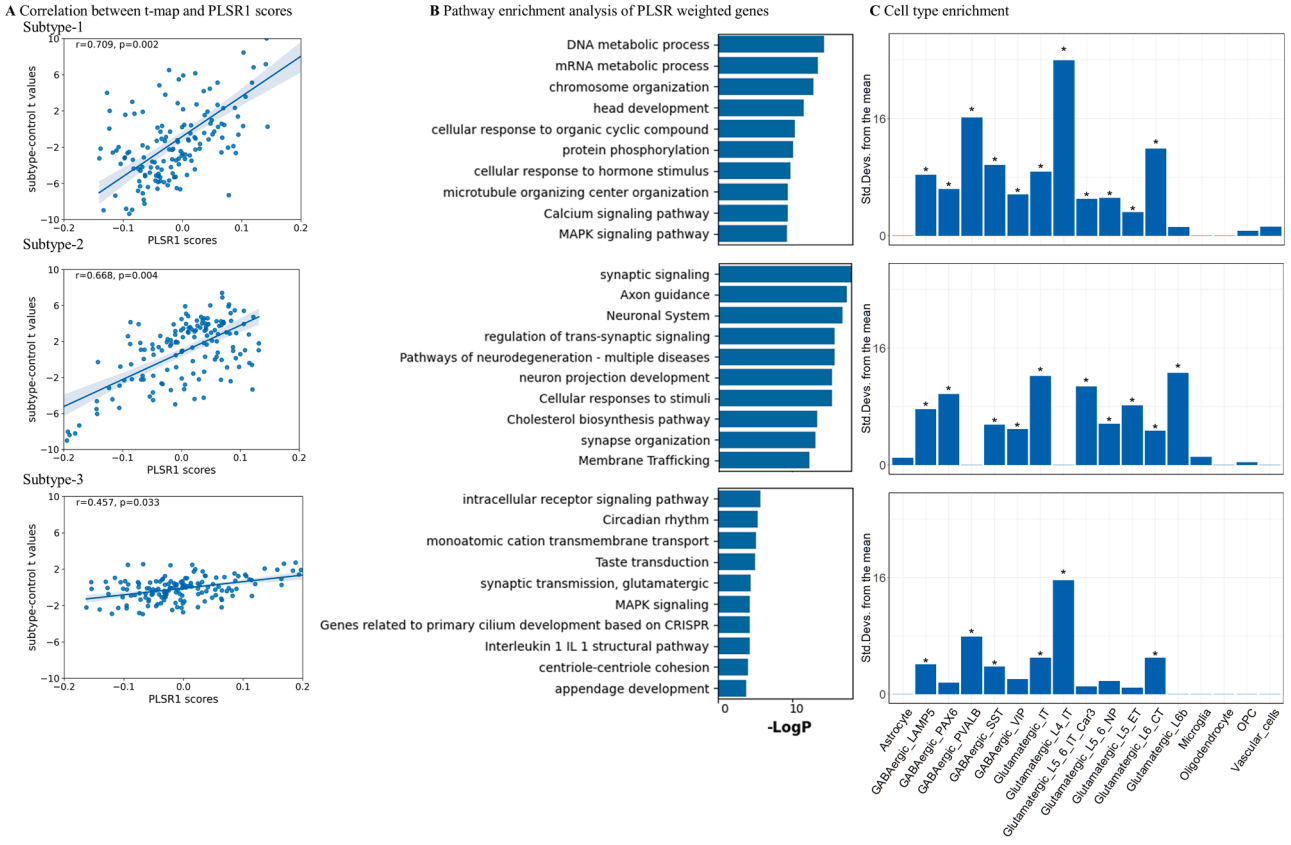

Fig. 4. Genetic analysis results. A. Correlation between case-control t-maps of regional MSN and PLSR1 scores in each subtype. **B.** Top ten significantly enriched Gene Ontology Biological Processes. **C.** Expression Weighted Cell Type Enrichment analysis results. Abbreviations: GABA, gamma-aminobutyric acid; LAMP5, lysosome-associated membrane glycoprotein 5; PAX6, Paired Box 6; PVALB, parvalbumin; SST, somatostatin; VIP, vasoactive intestinal peptide; L4, cortical layer 4; IT, intratelencephalic-projecting; CAR3, carbonic anhydrase 3 expressing; NP, near-projecting; ET, extratelencephalic-projecting; CT, corticothalamic; OPC, oligodendrocyte progenitor cells.

4. Discussion

To understand the structural network heterogeneity of ASD, we leveraged MSN and hierarchical clustering to test the presence of neuroimaging-defined subtypes in a cross-sectional sample of ASD. The first principal component of MSN was negatively correlated to communication, social and RRB symptoms, suggesting that morphometric similarity carries significance in ASD symptomology.

We identified three subtypes of ASD with unique patterns in structural similarity, functional connectivity, behavioral symptoms, and genetic underpinnings. Compared to TD, subtype-1 exhibited lower MSN association regions and higher MSN values in visual regions, while subtype-2 had higher MSN values in association regions and lower MSN values in visual regions. Subtype-3 exhibited morphometric similarity patterns largely comparable to TD, with minimal significant differences. Subtype-1, characterized by lower values of morphometric similarity in association regions, exhibited the most severe deficits and most atypical patterns of functional connectivity.

MSN captures inter-regional correlations across multiple morphometric features and has been reported to have a close relationship to axon connections and the reflection of diverse cognitive domains. The observed negative correlation between the first MSN component and

clinical metrics in ASD suggests that individuals with lower structural similarity across brain regions may exhibit more severe symptoms. The results from the subtypes are in line with this interpretation. The subtype with the most severe behavior symptoms, subtype-1, exhibited lower structural similarity in associative regions that support language, attention and social functions. For example, superior temporal and inferior frontal regions, which underlie language functions, showed high morphometric similarity values in TD but weaker similarity values in subtype-1. Similarly, the lateral parietal and anterior temporal regions of the default network, which support social cognitive functions like mentalizing, showed high morphometric similarity values in TD but weaker similarity values in subtype-1. Regions associated with attention, such as the dorsolateral prefrontal cortex, insula and medial frontal cortex also showed this similar pattern. It is possible that structural connectivity in these association regions is weakened in ASD subtype-1, contributing to the deficits in communication and social impairments.

Network-based subtyping in ASD has been largely driven by FC, with prior studies identifying subgroups differing in network segregation, integration, and individualized connectivity patterns across large-scale systems such as the default mode, cingulo-opercular, sensorimotor, and visual networks. These findings highlight that ASD is best characterized not by focal abnormalities but by distributed network-level alterations. However, whether analogous forms of heterogeneity exist at the level of structural network architecture has remained unclear. Using MSN, our results support the notion that ASD is a condition with large-scale network abnormalities. Most regions where subtype-1 differed from TD play important roles in ASD symptomatology. For instance, the middle and superior frontal cortices are part of the prefrontal cortex and are critical for executive functions, including working memory, rule learning, and planning (Badre and D'esposito, 2009; Harika-Germaneau et al., 2022). The inferior frontal, superior and middle temporal cortices have been characterized by language and multisensory processing (Stevenson et al., 2016; Fan et al., 2017; Petrides, 2023). The lateral occipital cortex is related to object recognition, facial recognition, and motion perception (Palejwala et al., 2020). Differences in these regions have been reported in individuals with ASD compared to typically developing people, including anatomical (Bigler et al., 2007; Chandran et al., 2021) and functional analysis (Delmonte et al., 2013; Jao Keehn et al., 2017; Jung et al., 2019; Xu et al., 2020). Our findings further suggested that the underlying structural connectivity of the association regions, as measured by MSN, may be weakened in the subgroup of ASD individuals with more severe communication and social symptoms. Interestingly, in the TD group, the occipital regions showed the lowest (negative) structural similarity values across the cortex, suggesting differentiation from other brain regions. In subtype-1, this differentiation is perhaps weakened, as indicated by less negative MSN values in these regions.

Intrinsic functional connectivity analyses revealed the atypical connections in subtype-1 and subtype-2, particularly in networks subserving social, attention, and language functions. Inter-network connectivity was strengthened in subtype-1 for the salience and visual network, and the language and visual networks. This finding of the stronger connectivity between salience and visual networks aligns with reports in school-age children with ASD (Alamdari et al., 2022; Girault et al., 2025). Girault et al. additionally reported that such hyperconnectivity is associated with higher levels of social affect impairment. The stronger connectivity between the language and visual networks is consistent with the findings by B. R. Morgan et al. (2019), who suggested that such abnormal connectivity may be particularly relevant to understanding the neurobiological underpinnings of language deficits in ASD. In subtype-2, connectivity between the default and salience network was elevated, which typically presents as anticorrelations and is important for attention control (Chai et al., 2012). This reduced anticorrelation might contribute to the more severe symptoms related to attention in subtype-2. Greater connectivity between these regions predicts greater social symptom severity on the social responsiveness scale (Chen et al., 2022). These findings are again compatible with the idea that ASD is characterized by abnormalities of distributed functional networks, rather than focal impairment (Wang et al., 2019). For instance, the default network contributes to internally-oriented processes that include mentalizing, theory of mind, and self-referential processing and plays an important role in the symptomatology of ASD (Padmanabhan et al., 2017). Reduced salience network integrity has been associated with sensory and socio-communicative symptoms (Abbott et al., 2016). Individuals with ASD show a reduced ability to integrate visual or multi-sensory feedback during motor behavior (Lepping et al., 2022), and are more reliant on visualization to support language comprehension (Kana et al., 2006). Our findings of the abnormal connectivity in the salience, default, language, and visual networks in the behaviorally more severe subtype-1 are consistent with these previous reports.

Different structural metrics reflect different facets of the brain and provide complementary information about understanding the cerebral cortex. The radial unit hypothesis of cortical development argues that neurons are arranged in columns from the inside to the outside of the cortex, and each such column acts as a computational unit (Mountcastle, 1998). SA is determined by the number of radial columns, where the number of columns is determined by the number of founder cells in the ventricular zone, and CT is determined by the number of cells within a column (Rakic, 1995; Mountcastle, 1998). GM is defined as the product of cortical thickness and surface area, and the group differences in GM could be caused by the independent changes in SA and CT, or the degree of folding (Wagstyl and Lerch, 2018). On the other hand, the development of SA may also be related to changes in gyrification, while the developmental changes in gyrification are related to changes in curvature, which are affected by both changes in folding frequency or changes in folding magnitude (Wierenga et al., 2014). In short, the metrics of the brain are interdependent on the morphology of the brain; therefore, it is critical to consider the correlations of different structural measurements to accurately characterize morphological changes (Wagstyl and Lerch, 2018). By considering each of these structural features, morphometric similarity–based structural network measures revealed large-scale, network-level differences between ASD subtypes with mild and severe symptoms.

DTI-based tractography is affected by crossing-fiber ambiguity, where a single tensor cannot resolve multiple fiber orientations within a voxel, and distance- and gyral-related biases, leading to underestimation of long-range pathways and premature termination near gyral crowns. By contrast, MSN does not rely on fiber tracking and is therefore less vulnerable to these sources of variability, while providing a biologically meaningful measure of cortical similarity that has been shown to correspond to cytoarchitectonic gradients and transcriptomic organization. In addition, prior studies using a wide range of parcellations—from coarse anatomical atlases (68 parcels) to high-resolution functional and equal-area parcellations (308–1533 parcels)—consistently report highly similar morphometric similarity (Seidlitz et al., 2018; Li et al., 2024; Del Casale et al., 2025; Tranfa et al., 2025). These findings indicate that MSN-derived network organization is largely robust to parcellation choice.

The transcriptomic analysis revealed genetic differences related to the structural atypicality of the subtypes. Notably enriched cell types included GABAergic PVALB, glutamatergic intratelencephalic L4_IT and L6b neurons. The GABAergic PVALB neurons affect the neuronal functions and dynamics by adjusting buffering calcium (Lawrence et al., 2010; Filice et al., 2016). The involvement of glutamatergic intratelencephalic (IT) neurons in ASD is supported by findings that the receptor tyrosine kinase MET, an autism risk allele, is expressed in IT neurons, and carriers show atypical activation or deactivation responses to social stimuli (Shepherd, 2013). Glutamatergic L6b are crucial for establishing the circuits for sensory processing early in development, and work as a prime position to monitor bidirectional information transfer between the cortex and thalamus (Zolnik et al., 2020). In addition, gene-marker-based analysis implicates the significant

enrichment of layer 5/6 glutamatergic projection neurons in ASD (Willsey et al., 2013). These results suggest distinct genetic signatures among the three subtypes.

The current study has several limitations. First, subtype-3 exhibited morphometric similarity patterns that closely resembled those of typically developing controls. This subgroup may represent individuals with minimal deviation from the normative range rather than a distinct neuroanatomical subtype. Similar "catch-all" clusters have been reported in previous subtyping studies of ASD and other neurodevelopmental conditions, often reflecting variance that is more continuous than categorical. Future work using normative or dimensional modeling frameworks could better characterize such subtle, individualized deviations and provide a more continuous representation of autism-related brain variation. Second, the dataset contained limited data on behavior/symptoms, which may constrain the interpretation of brain–behavior relationships. These brain structural network-based subtypes may differ in other behavioral dimensions not captured by ADI-R. Third, the present study included only male participants due to the limited number of females available in the dataset and known sex-related differences in autism prevalence and neuroanatomy. Therefore, the generalizability of our findings to females with ASD remains to be tested. Given well-established sex differences in autism prevalence and neurobiology, future work should aim to replicate these findings in female samples to determine whether similar subtype patterns exist in females with ASD. In addition, incorporating longitudinal designs and more comprehensive behavioral assessments will be important to evaluate the developmental stability and behavioral relevance of the identified subtypes. Finally, our study adopts this established approach to explore the potential molecular substrates associated with the observed MSN-based alterations in ASD, without inferring direct case–control differences in gene expression. Importantly, we acknowledge that AHBA-based analyses provide indirect molecular inference and cannot determine ASD-specific transcriptional changes.

In conclusion, using an advanced structural network mapping approach, we found three distinct MRI subtypes characterized by different patterns of structural network as measured by MSN, behavioral, functional connectivity, and genetic profiles. Weaker morphometric similarity in association regions is associated with an ASD subtype with more severe social and language symptoms. These findings could aid in advancing personalized medicine or other intervention approaches in ASD.

Data availability

ABIDE: https://fcon_1000.projects.nitrc.org/indi/abide/
POND: https://pond-network.ca/
HCP-D: https://www.humanconnectome.org/study/hcp-lifespan-development
AHBA: https://human.brain-map.org/static/brainexplorer

Code availability

The code used in this study is available from the corresponding author upon reasonable request.

Acknowledgments and disclosures

This work was supported by Canada First Research Excellence Fund, awarded to McGill University for the Healthy Brains for Healthy Lives initiative (XJC), the Canada Research Chairs program (XJC), Canadian Institute of Health Research (CIHR PAU-185726; XJC), and Brain Canada. H.J. is funded by the China Scholarship Council (CSC No. 201906070288).

CRediT authorship contribution statement

Hongxiu Jiang: Writing – review & editing, Writing – original draft, Visualization, Validation, Supervision, Software, Resources, Project administration, Methodology, Investigation, Formal analysis, Data curation, Conceptualization. **Raul Rodriguez-Cruces:** Methodology. **Ke Xie:** Writing – review & editing, Methodology. **Valeria Kebets:** Writing – review & editing, Methodology. **Yezhou Wang:** Methodology. **Clara F. Weber:** Writing – review & editing, Methodology. **Ying He:** Writing – review & editing, Methodology. **Jonah Kember:** Methodology. **Hilary Sweatman:** Writing – review & editing, Methodology. **Zeus Gracia Tabuenca:** Data curation. **Jean-Baptiste Poline:** Writing – review & editing, Methodology. **Danilo Bzdok:** Writing – review & editing, Methodology. **Seok-Jun Hong:** Writing – review & editing. **Boris Bernhardt:** Methodology. **Xiaoqian Chai:** Writing – review & editing, Project administration, Methodology, Funding acquisition, Conceptualization.

Declaration of competing interest

The authors declare no conflict of interest.

Supplementary materials

Supplementary material associated with this article can be found, in the online version, at doi:10.1016/j.neuroimage.2026.121775.

References

Abbott, A.E., 2016. Patterns of atypical functional connectivity and behavioral links in autism differ between default, salience, and executive networks. Cereb. Cortex 26 (10), 4034–4045.
Alamdari, S.B., 2022. Cognitive theories of autism based on the interactions between brain functional networks. Front. Hum. Neurosci. 16, 828985.
Alexander-Bloch, A.F., 2018. On testing for spatial correspondence between maps of human brain structure and function. Neuroimage 178, 540–551.
Arnatkevičiūtė, A., 2019. A practical guide to linking brain-wide gene expression and neuroimaging data. Neuroimage 189, 353–367.
Badre, D., D'esposito, M., 2009. Is the rostro-caudal axis of the frontal lobe hierarchical? Nat. Rev. Neurosci. 10 (9), 659–669.
Balardin, J.B., 2015. Decreased centrality of cortical volume covariance networks in autism spectrum disorders. J. Psychiatr. Res. 69, 142–149.
Behzadi, Y., 2007. A component based noise correction method (CompCor) for BOLD and perfusion based fMRI. Neuroimage 37 (1), 90–101.
Benjamini, Y., Hochberg, Y., 1995. Controlling the false discovery rate: a practical and powerful approach to multiple testing. J. R. Stat. Soc.: Ser. B 57 (1), 289–300.
Bigler, E.D., 2007. Superior temporal gyrus, language function, and autism. Dev. Neuropsychol. 31 (2), 217–238.
Bridges Jr, C.C., 1966. Hierarchical cluster analysis. Psychol. Rep. 18 (3), 851–854.
Calhoun, V.D., 2001. A method for making group inferences from functional MRI data using independent component analysis. Hum. Brain Mapp. 14 (3), 140–151.
Cao, H., 2023. The alteration of cortical microstructure similarity in drug-resistant epilepsy correlated with mTOR pathway genes. EBioMedicine 97.
Carroll, L., 2021. Autism spectrum disorders: multiple routes to, and multiple consequences of, abnormal synaptic function and connectivity. Neuroscientist 27 (1), 10–29.
Chai, X.J., 2012. Anticorrelations in resting state networks without global signal regression. Neuroimage 59 (2), 1420–1428.
Chandran, V.A., 2021. Brain structural correlates of autistic traits across the diagnostic divide: a grey matter and white matter microstructure study. NeuroImage: Clin. 32, 102897.
Chen, H., 2019. Parsing brain structural heterogeneity in males with autism spectrum disorder reveals distinct clinical subtypes. Hum. Brain Mapp. 40 (2), 628–637.
Chen, R., 2011. Structural MRI in autism spectrum disorder. Pediatr. Res. 69 (8), 63–68.
Chen, S., 2017. Latent and abnormal functional connectivity circuits in autism spectrum disorder. Front. Neurosci. 11, 125.
Chen, Y.-Y., 2022. Excessive functional coupling with less variability between salience and default mode networks in autism spectrum disorder. Biol. Psychiatry: Cogn. Neurosci. Neuroimaging 7 (9), 876–884.
Choi, H., 2022. Diagnosis-informed connectivity subtyping discovers subgroups of autism with reproducible symptom profiles. Neuroimage, 119212.
Cruz Puerto, M., Sandín Vázquez, M., 2024. Understanding heterogeneity within autism spectrum disorder: a scoping review. Adv. Autism 10 (4), 314–322.
Dean III, D.C., 2016. Investigating the microstructural correlation of white matter in autism spectrum disorder. Brain Connect. 6 (5), 415–433.
Del Casale, A., 2025. Multimodal morphometric similarity network analysis of autism spectrum disorder. Brain Sci. 15 (3), 247.

Delmonte, S., 2013. Functional and structural connectivity of frontostriatal circuitry in autism spectrum disorder. Front. Hum. Neurosci. 7, 430.
Desikan, R.S., 2006. An automated labeling system for subdividing the human cerebral cortex on MRI scans into gyral based regions of interest. Neuroimage 31 (3), 968–980.
Di Martino, A., 2014. The autism brain imaging data exchange: towards a large-scale evaluation of the intrinsic brain architecture in autism. Mol. Psychiatry 19 (6), 659–667.
Di Martino, A., 2017. Enhancing studies of the connectome in autism using the autism brain imaging data exchange II. Sci. Data 4 (1), 1–15.
Dorfschmidt, L., 2024. Human adolescent brain similarity development is different for paralimbic versus neocortical zones. Proc. Natl. Acad. Sci. 121 (33), e2314074121.
Easson, A.K., 2019. Functional connectivity-based subtypes of individuals with and without autism spectrum disorder. Netw. Neurosci. 3 (2), 344–362.
Fan, J., 2017. Spontaneous neural activity in the right superior temporal gyrus and left middle temporal gyrus is associated with insight level in obsessive-compulsive disorder. J. Affect. Disord. 207, 203–211.
Fenchel, D., 2022. Neonatal multi-modal cortical profiles predict 18-month developmental outcomes. Dev. Cogn. Neurosci. 54, 101103.
Filice, F., 2016. Reduction in parvalbumin expression not loss of the parvalbumin-expressing GABA interneuron subpopulation in genetic parvalbumin and shank mouse models of autism. Mol. Brain 9, 1–17.
Fortin, J.-P., 2018. Harmonization of cortical thickness measurements across scanners and sites. Neuroimage 167, 104–120.
Girault, J.B., 2025. Functional connectivity between the visual and salience networks and autistic social features at school-age. J. Neurodev. Disord. 17 (1), 1–11.
Goulas, A., 2017. Principles of ipsilateral and contralateral cortico-cortical connectivity in the mouse. Brain Struct. Funct. 222 (3), 1281–1295.
Guo, X., 2022. Inter-individual heterogeneity of functional brain networks in children with autism spectrum disorder. Mol. Autism 13 (1), 1–13.
Harika-Germaneau, G., 2022. Baseline clinical and neuroimaging biomarkers of treatment response to high-frequency rTMS over the left DLPFC for resistant depression. Front. Psychiatry 13, 894473.
Hawrylycz, M.J., 2012. An anatomically comprehensive atlas of the adult human brain transcriptome. Nature 489 (7416), 391–399.
Hong, S.-J., 2018. Multidimensional neuroanatomical subtyping of autism spectrum disorder. Cereb. Cortex 28 (10), 3578–3588.
Hyde, K.L., 2010. Neuroanatomical differences in brain areas implicated in perceptual and other core features of autism revealed by cortical thickness analysis and voxel-based morphometry. Hum. Brain Mapp. 31 (4), 556–566.
Jao Keehn, R.J., 2017. Impaired downregulation of visual cortex during auditory processing is associated with autism symptomatology in children and adolescents with autism spectrum disorder. Autism Res. 10 (1), 130–143.
Jung, M., 2019. Decreased structural connectivity and resting-state brain activity in the lateral occipital cortex is associated with social communication deficits in boys with autism spectrum disorder. Neuroimage 190, 205–212.
Kana, R.K., 2006. Sentence comprehension in autism: thinking in pictures with decreased functional connectivity. Brain 129 (9), 2484–2493.
Khundrakpam, B.S., 2017. Cortical thickness abnormalities in autism spectrum disorders through late childhood, adolescence, and adulthood: a large-scale MRI study. Cereb. Cortex 27 (3), 1721–1731.
Lawrence, Y., 2010. Parvalbumin-, calbindin-, and calretinin-immunoreactive hippocampal interneuron density in autism. Acta Neurol. Scand. 121 (2), 99–108.
Lenroot, R.K., Yeung, P.K., 2013. Heterogeneity within autism spectrum disorders: what have we learned from neuroimaging studies? Front. Hum. Neurosci. 7, 733.
Lepping, R.J., 2022. Visuomotor brain network activation and functional connectivity among individuals with autism spectrum disorder. Hum. Brain Mapp. 43 (2), 844–859.
Li, J., 2021. Cortical structural differences in major depressive disorder correlate with cell type-specific transcriptional signatures. Nat. Commun. 12 (1), 1–14.
Li, J., 2024. Morphometric brain organization across the human lifespan reveals increased dispersion linked to cognitive performance. PLoS Biol. 22 (6), e3002647.
Li, W., 2017. Construction of individual morphological brain networks with multiple morphometric features. Front. Neuroanat. 11, 34.
Lombardo, M.V., 2019. Big data approaches to decomposing heterogeneity across the autism spectrum. Mol. Psychiatry 24 (10), 1435–1450.
London, E.B., 2014. Categorical diagnosis: a fatal flaw for autism research? Trends. Neurosci. 37 (12), 683–686.
Markello, R.D., 2021. Standardizing workflows in imaging transcriptomics with the abagen toolbox. Elife 10, e72129.
Morgan, B.R., 2019. Characterization of autism spectrum disorder across the age span by intrinsic network patterns. Brain Topogr. 32 (3), 461–471.
Morgan, S.E., 2019. Cortical patterning of abnormal morphometric similarity in psychosis is associated with brain expression of schizophrenia-related genes. Proc. Natl. Acad. Sci. 116 (19), 9604–9609.
Mountcastle, V.B., 1998. Perceptual Neuroscience: The Cerebral Cortex. Harvard University Press.
Padmanabhan, A., 2017. The default mode network in autism. Biol. Psychiatry: Cogn. Neurosci. Neuroimaging 2 (6), 476–486.
Palejwala, A.H., 2020. Anatomy and white matter connections of the lateral occipital cortex. Surg. Radiol. Anat. 42, 315–328.
Petrides, M., 2023. On the evolution of polysensory superior temporal sulcus and middle temporal gyrus: a key component of the semantic system in the human brain. J. Comp. Neurol. 531 (18), 1987–1995.
Pua, E.P.K., 2017. Autism spectrum disorders: neuroimaging findings from systematic reviews. Res. Autism Spectr. Disord. 34, 28–33.
Rakic, P., 1995. A small step for the cell, a giant leap for mankind: a hypothesis of neocortical expansion during evolution. Trends Neurosci. 18 (9), 383–388.
Rodríguez-Cruces, R., 2020. Multidimensional associations between cognition and connectome organization in temporal lobe epilepsy. Neuroimage 213, 116706.
Romero-Garcia, R., 2012. Effects of network resolution on topological properties of human neocortex. Neuroimage 59 (4), 3522–3532.
Rousseeuw, P.J., 1987. Silhouettes: a graphical aid to the interpretation and validation of cluster analysis. J. Comput. Appl. Math. 20, 53–65.
Sebenius, I., 2024. Structural MRI of brain similarity networks. Nat. Rev. Neurosci. 1–18.
Seidlitz, J., 2018. Morphometric similarity networks detect microscale cortical organization and predict inter-individual cognitive variation. Neuron 97 (1), 231–247 e237.
Sharda, M., 2016. Disruption of structural covariance networks for language in autism is modulated by verbal ability. Brain Struct. Funct. 221 (2), 1017–1032.
Shepherd, G.M., 2013. Corticostriatal connectivity and its role in disease. Nat. Rev. Neurosci. 14 (4), 278–291.
Skene, N.G., Grant, S.G., 2016. Identification of vulnerable cell types in major brain disorders using single cell transcriptomes and expression weighted cell type enrichment. Front. Neurosci. 10, 16.
Somerville, L.H., 2018. The Lifespan Human Connectome Project in Development: a large-scale study of brain connectivity development in 5–21 year olds. Neuroimage 183, 456–468.
Stevenson, R.A., 2016. Keeping time in the brain: autism spectrum disorder and audiovisual temporal processing. Autism Res. 9 (7), 720–738.
Tranfa, M., 2025. Conventional MRI-based structural disconnection and morphometric similarity networks and their clinical correlates in multiple sclerosis. Neurology 104 (4), e213349.
Valk, S.L., 2015. Multicenter mapping of structural network alterations in autism. Hum. Brain Mapp. 36 (6), 2364–2373.
Vuksanović, V., 2022. Brain morphometric similarity and flexibility. Cereb. Cortex. Commun. 3 (3), tgac024.
Wagstyl, K., Lerch, J.P., 2018. Cortical thickness. Brain Morphometry. Springer, pp. 35–49.
Wang, Z., 2019. Resting-state brain network dysfunctions associated with visuomotor impairments in autism spectrum disorder. Front. Integr. Neurosci. 13, 17.
Whitfield-Gabrieli, S., Nieto-Castanon, A., 2012. Conn: a functional connectivity toolbox for correlated and anticorrelated brain networks. Brain Connect. 2 (3), 125–141.
Wierenga, L.M., 2014. Unique developmental trajectories of cortical thickness and surface area. Neuroimage 87, 120–126.
Willsey, A.J., 2013. Coexpression networks implicate human midfetal deep cortical projection neurons in the pathogenesis of autism. Cell 155 (5), 997–1007.
Wold, H., 1966. Estimation of principal components and related models by iterative least squares. Multivar. Anal. 391–420.
Wold, S., 1987. Principal component analysis. Chemom. Intell. Lab. Syst. 2 (1–3), 37–52.
Wu, X., 2023. Morphometric dis-similarity between cortical and subcortical areas underlies cognitive function and psychiatric symptomatology: a preadolescence study from ABCD. Mol. Psychiatry 28 (3), 1146–1158.
Xu, J., 2020. Specific functional connectivity patterns of middle temporal gyrus subregions in children and adults with autism spectrum disorder. Autism Res. 13 (3), 410–422.
Zabihi, M., 2020. Fractionating autism based on neuroanatomical normative modeling. Transl. Psychiatry 10 (1), 1–10.
Zhou, Y., 2019. Metascape provides a biologist-oriented resource for the analysis of systems-level datasets. Nat. Commun. 10 (1), 1–10.
Zolnik, T.A., 2020. Layer 6b is driven by intracortical long-range projection neurons. Cell Rep. 30 (10), 3492–3505.e3495.